Engineering Atomically Dispersed Single Cu-N_3 Catalytic Sites for Highly Selective Oxidation of Benzene to Phenol

Yitao Zhao[+], Haoran Xing[+], Qiang Wang, Yinjuan Chen, Jiawei Xia, Hui Xu, Guangyu He, Fengxiang Yin, Qun Chen*, Haiqun Chen*

Jiangsu Key Laboratory of Advanced Catalytic Materials and Technology, Advanced Catalysis and Green Manufacturing Collaborative Innovation Center, School of Petrochemical Engineering, Changzhou University, Changzhou, 213164, China

Corresponding Authors:

E-mail: chenhq@cczu.edu.cn; chenqunjpu@yahoo.com.

+ Yitao Zhao and Haoran Xing contributed equally.

Table of Contents

MATERIALS AND METHODS

Materials and regents

Pure copper mesh (300 mesh, T1 Cu > 99.9%, CP) was purchased from Yingtan Zhongzhen Copper Co., Ltd. Dicyandiamide (DCDA, > 99%, AR.), acetonitrile (MeCN, >99%, AR.), methanol (MeOH, > 99%, AR.), N, N-Dimethylformamide (DMF, 99%, AR.), dimethyl sulfoxide (DMSO, > 99%, AR.), acetone (> 99%, AR.), n-etradecane (99%, AR.), sulfuric acid (H_2SO_4, > 98%, AR.), benzene (C_6H_6, > 99%, AR.), hydrogen peroxide solution (H_2O_2, 35%, AR.) were bought from Sino pharm Chemical Reagent Co., Ltd. (China). All chemicals were used as received without any further purification unless stated otherwise. The deionized·(DI)·water was obtained from an ULUPURE system (2.06 MΩ·cm resistivity) and used throughout the whole experiment.

Synthesis of SA_xCu-NRGO catalysts

Graphite oxide (GO) was first synthesized according to the modified Hummer's method. [1] The N-doped reduced graphene oxide (NRGO) based single-atom Cu catalyst (SACu-NRGO) were prepared via one–pot pyrolysis of the mixture of DCDA and GO with different mass ratios at high temperature, where the single-atom Cu species was originated from the Cu mesh wrapped around the mixture reactant. As schematically illustrated in Figure 1a, 100 mL of GO aqueous suspension (2 mg mL^{-1}) and 3.6 g of DCDA were first mixed under continuous stirring for 10 h, followed by freeze-drying to obtain a homogeneous mixture, marked as DCDA&GO. The solid mixture was then carefully wrapped with one layer of Cu mesh and placed in a partially covered quartz boat with a quartz plate to avoid contamination. Afterwards, the quartz boat was inserted in a tube furnace for sequential pyrolysis at 600 °C for 2 h and 800 °C for1 h, respectively, under flowing N_2 with the same heating rate of 2 °C min^{-1}. Upon cooling down naturally to room temperature, the solid residue in the quartz boat, labelled as Cu-NRGO, was dispersed in H_2SO_4 aqueous solution (0.5 mol L^{-1}) and held at 80 °C for 10 h to remove Cu nanoparticles. After washing with DI water until neutral and drying in the vacuum oven at 80 °C, the single atomic Cu catalyst supported on NRGO was obtained, labelled as SA_xCu-NRGO (x = 0, 3, 6, 9, 12, 15, 18 and 21, which represents

the corresponding DCDA&GO mass ratios of 0/1, 3/1, 6/1, 9/1, 12/1, 15/1, 18/1 and 21/1, respectively). For comparison, metal-free pristine N–doped reduced graphene oxide (NRGO) as the reference sample was also prepared following the same synthetic procedure, but without the participance of Cu mesh.

Characterization

The morphologies of the catalysts were observed by field emission scanning electron microscopy (FESEM, Zeiss, SUPRA55 SAPPHIRE) at an U_0 = 5 kV, transmission electron microscopy (TEM, JEM-2100, JEOL) at U_0 = 200 kV, and high-angle annular dark-field scanning transmission electron microscopy (HAADF-STEM, JEOL JEM-ARM200CF probe-aberration corrected microscope) at U_0 = 200 kV equipped with a cold field emission gun. The crystalline structures of the catalysts were obtained according to powder X-ray diffraction (XRD) patterns recorded on a Rigaku powder X-ray diffractometer using Ni-filtered CuKα radiation with 2θ ranging from 5 to 80°. Information about the functional groups and defects from the catalysts were characterized by Fourier transform infrared spectra (FTIR, Nicolet IS20), and Raman spectra (Renishaw InVia Raman microscope) with an excitation laser wavelength of 532 nm at room temperature. Chemical environment of each element in the catalysts was analyzed via X-ray photoelectron spectroscopy (XPS, PerkinElmer, BD upgraded, PHI-5000C ESCA system coupled with Auger spectrum) with Mg Kα radiation (hv = 1253.6 eV). Detailed chemical structures of the samples were further examined using Cu K-edge X-ray absorption near edge structure (XANES) and extended X-ray absorption fine structure (EXAFS) measurements, conducted at the HXMA beamline of the Taiwan Light Source. The apparent specific surface area and pore size distribution of the catalysts were measured on a Beishide 3H-2000PS2 analyzer at 77 K, where the values were obtained according to the isotherm data points of the nitrogen adsorption branch based on the Brunauer-Emmett-Teller (BET) model. The Cu content of each catalyst was measured by Thermogravimetric analysis (TGA, Q500) and Inductive coupled plasma (ICP) atomic emission spectrum (SHIMADZAU, ICPS-7510).

Catalytic Performance

The oxidation of benzene to phenol was employed as the model reaction to evaluate the catalytic performance of SA_xCu-NRGO catalysts. Typically, to a mixture in a 10 mL sealed round–bottom flask containing 2.0 mL of CH_3CN, 0.1 mL of benzene and 1.5 mL of H_2O_2 (30 wt%), 12.5 mg of the catalyst was added and dispersed homogeneously with the help of sonication. Then the flask was placed in a water bath at room temperature with continuous magnetic stirring to start the reaction. When the reaction was completed and cooled down to room temperature, the product was extracted with dichloromethane, and a certain amount of *n*-tetradecane was added as the internal standard. The yield and selectivity were analyzed on an Agilent 7820A gas chromatograph (GC) equipped with a 30 m × 0.32 mm × 0.25 μm HP-5 capillary column and a flame ionization detector (FID).

Density functional theoretical calculations

Density functional theoretical (DFT) calculations were performed by using the Perdew–Burke-Ernzerhof (PBE) functional within the formulation of generalized gradient approximation (GGA) as implemented in the Vienna ab initio simulation package. The Gamma meshes of 2 × 2 × 1 *k*-points sampling in the Brillouin zone was employed in all calculations of geometry optimization. The catalyst models were set in a 6 × 6 supercell of graphene, where the vacuum thickness between the catalyst slabs was set as 20 Å to get rid of the influence from the virtual interlayer interaction. Structural optimizations were conducted by using the Gaussian smearing finite-temperature broadening method (= 0.05 Hatree). To ensure high-quality results, the kinetic energy cut-off for the plane-wave basis sets was set as 400 eV. The energy criterion was set to be 10^{-6} eV in iterative solution of the Kohn–Sham equation. All the atoms were relaxed during the structure optimization until the maximum force on any ion was less than 0.01 eV $Å^{-1}$. The climbing-image nudged elastic band method was used to identify the transition states until the maximum force on any ion was less than 0.03 eV $Å^{-1}$. Vibrational frequency analysis was performed to gain the thermodynamic results. According to the vibrational analysis, the correlation of thermodynamic parameters (with the zero-point energy included) such as enthalpy (ΔH_{corr}), entropy (ΔS_{corr}) and free energy (ΔG_{corr}) were taken into consideration in the study of the

reaction mechanism. And the free energy at specific temperature were calculated by the formula $G = E_{total} + G_{corr}$, where E_{total} is the total energy of the specific moiety on the minimum energy path (MEP) and G_{corr} is the free-energy correlation with the zero-point energy included at the specific temperature. The related free energy change at 298.15 K in each step was calculated according to the equation $\Delta G = \Delta E_{total} + \Delta G_{corr}$, where ΔE_{total} is the energy difference of the total energy between each species, and ΔG_{corr} is the energy difference of the free energy.

Supplementary Figures

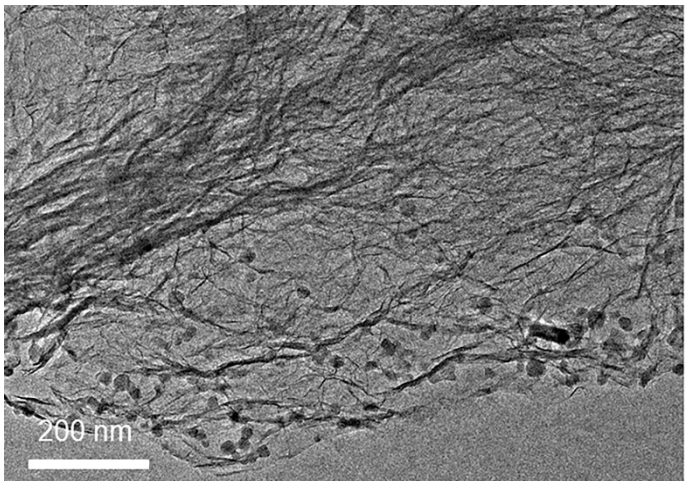

Fig. S1. TEM images of Cu-NRGO.

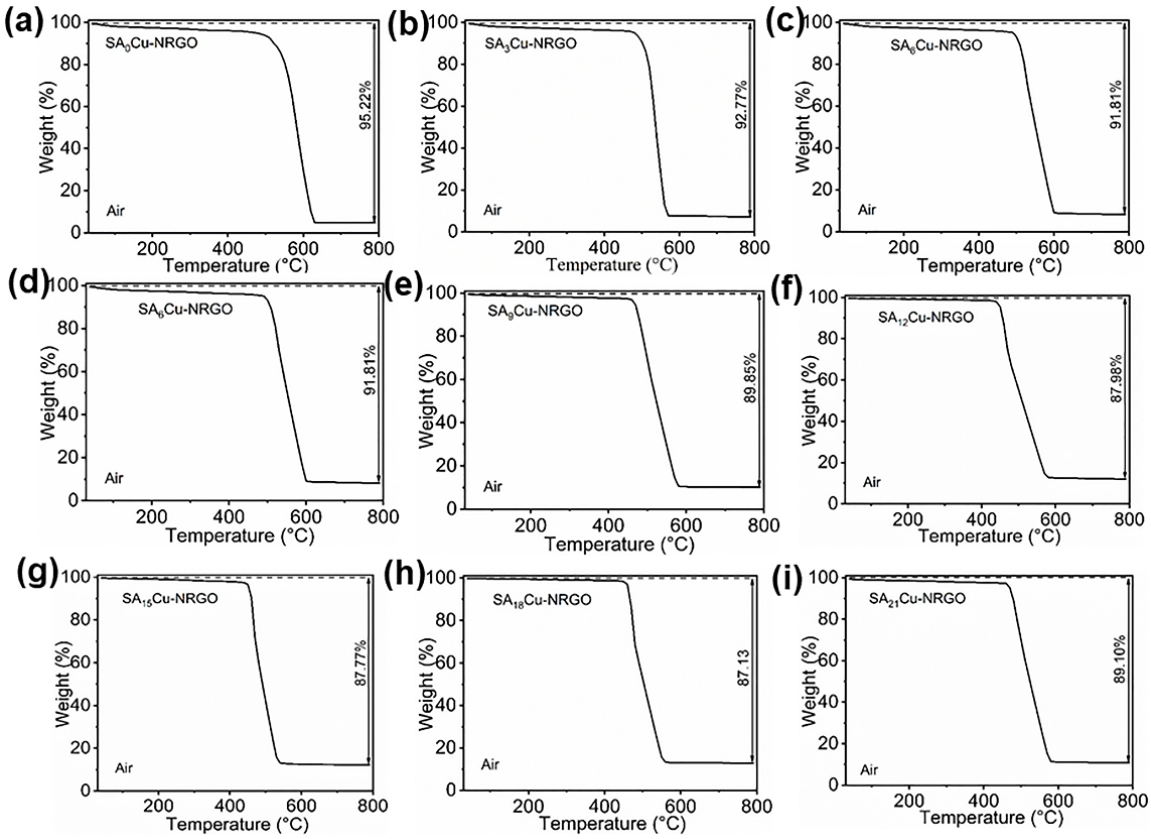

Fig. S2. TG results of all as-prepared samples.

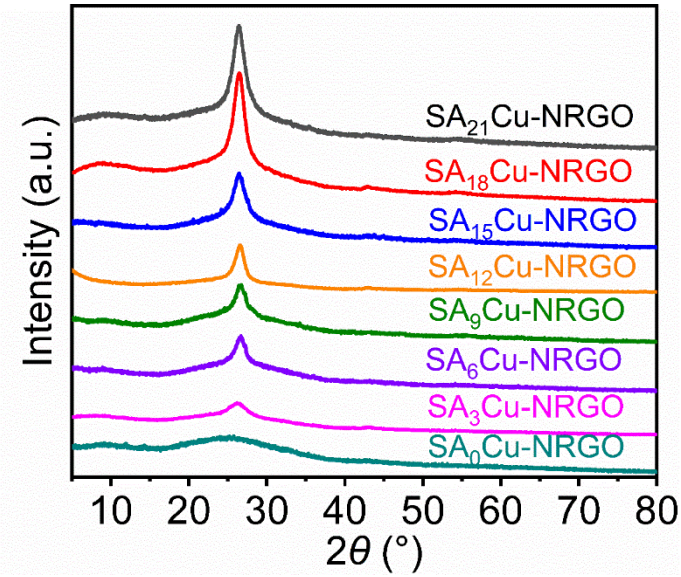

Fig. S3. XRD patterns of SA_xCu-NRGO.

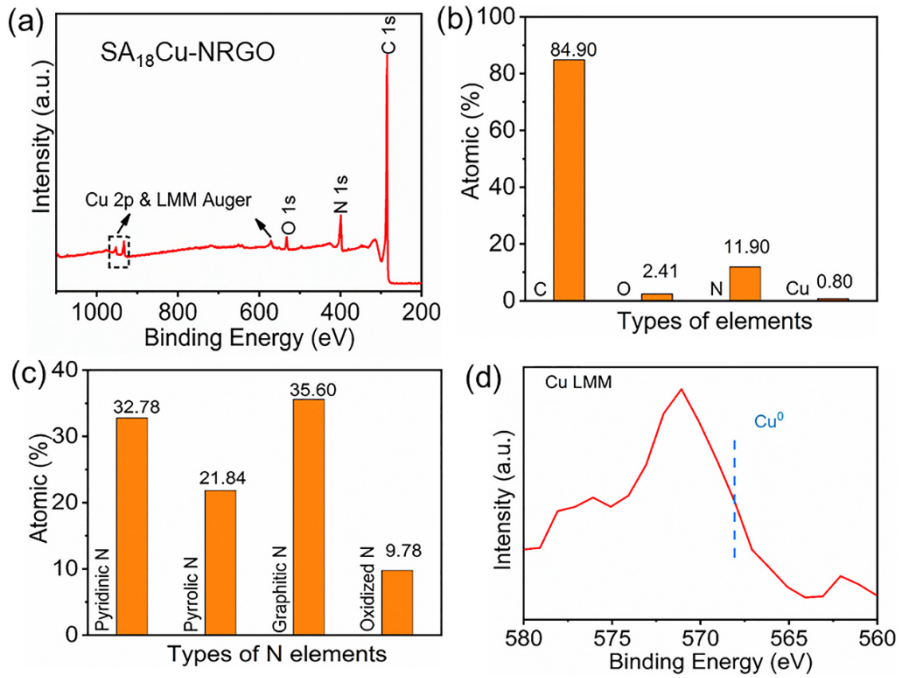

Fig. S4. XPS survey spectra (a), distribution of different elements (b), different types of N (c), and Cu LMM Auger spectrum (d) of SA_{18}Cu-NRGO.

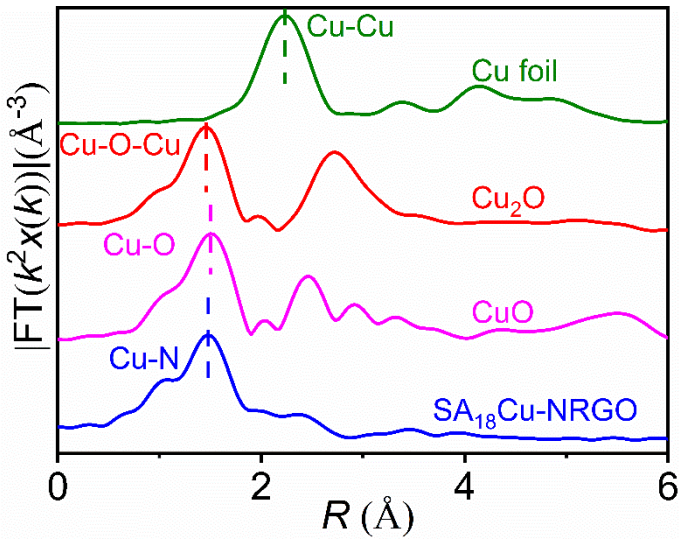

Fig. S5. The k^3-weighted Fourier transform spectra for Cu *K*-edge EXAFS of Cu foil, Cu_2O, CuO and SA_{18}Cu-NRGO.

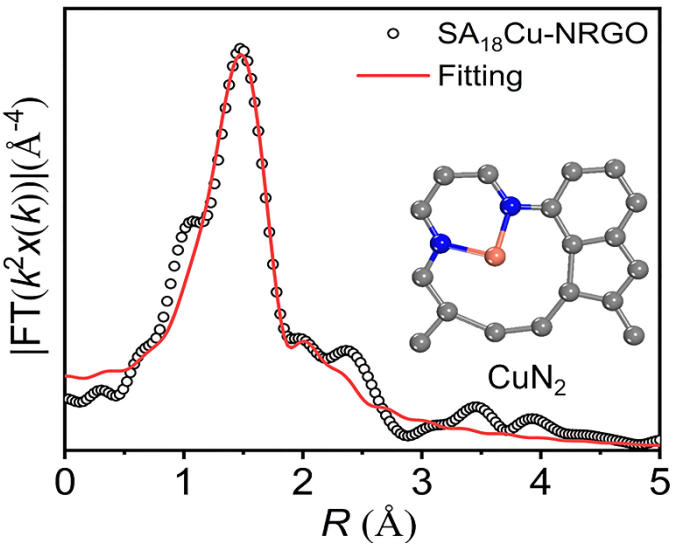

Fig. S6. EXAFS *R*-space fitting curve of $SA_{18}Cu$-NRGO with a CuN_2 structure as the inset.

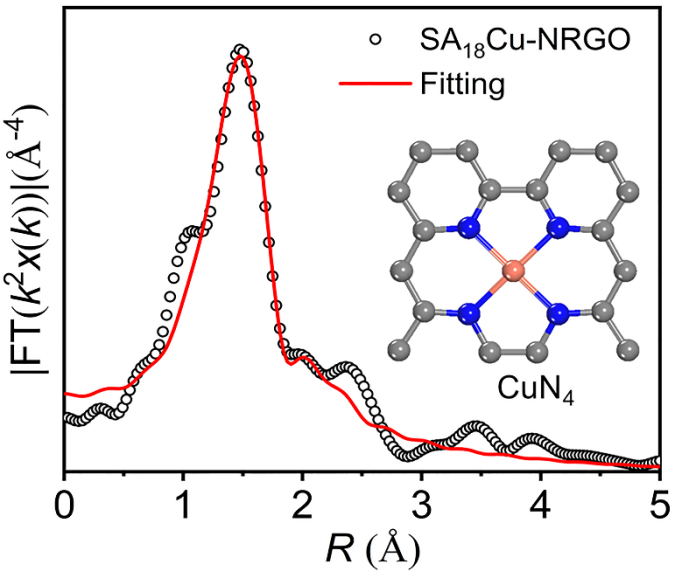

Fig. S7. EXAFS *R*-space fitting curves of $SA_{18}Cu$-NRGO with a CuN_4 structure as the inset.

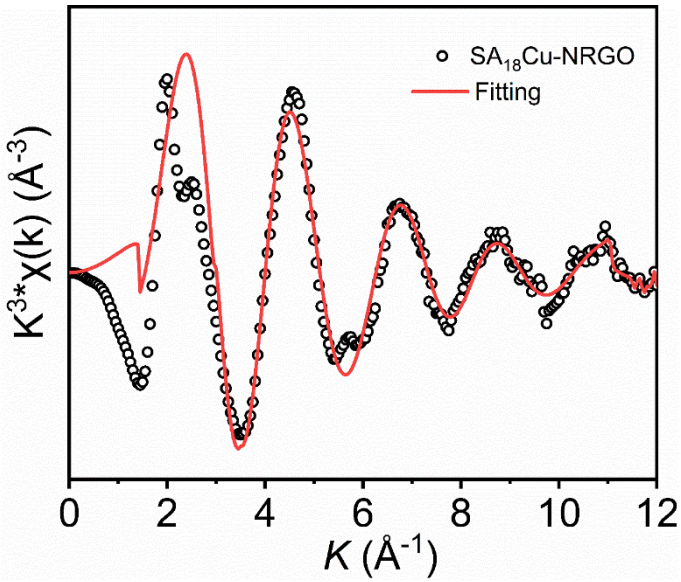

Fig. S8. EXAFS *k* space of SA_{18}Cu-NRGO.

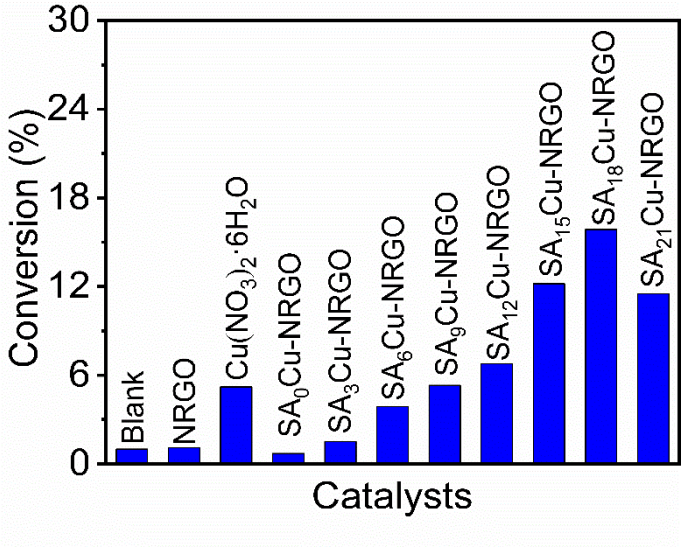

Fig. S9 The effect of different catalysts on the oxidation of benzene. (Reaction conditions: 12.5 mg of the sample, 0.1 mL of benzene, 2.0 mL of MeCN and 1.5 mL of H_2O_2, reaction for 24 h at 25 ^oC.)

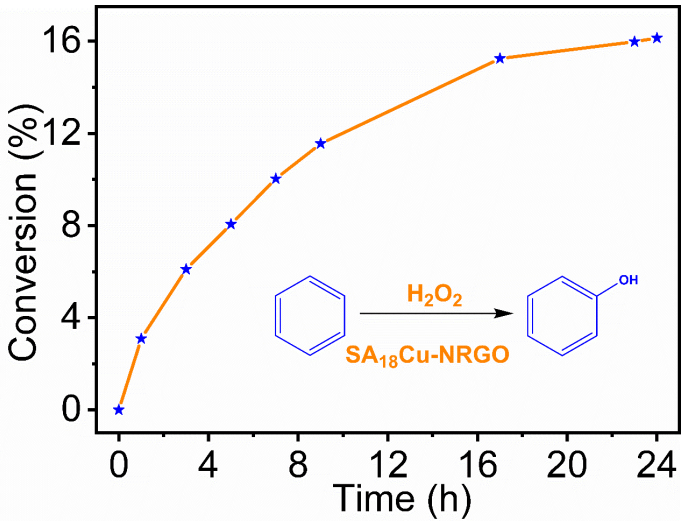

Fig. S10. The effect of reaction time on the oxidation of benzene. (Reaction conditions: 12.5 mg of the sample, 0.1 mL of benzene, 1.5 mL of solvent, and 1.5 mL of H_2O_2, reaction for 24 h at 25 °C.)

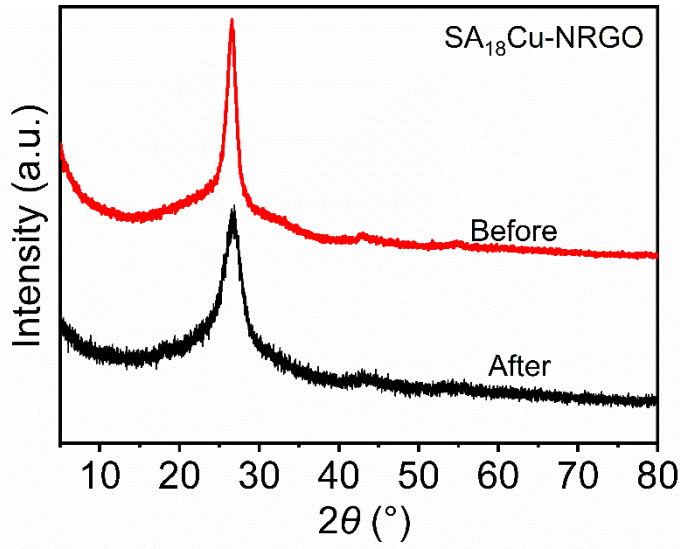

Fig. S11. XRD patterns before and after the oxidation of benzene.

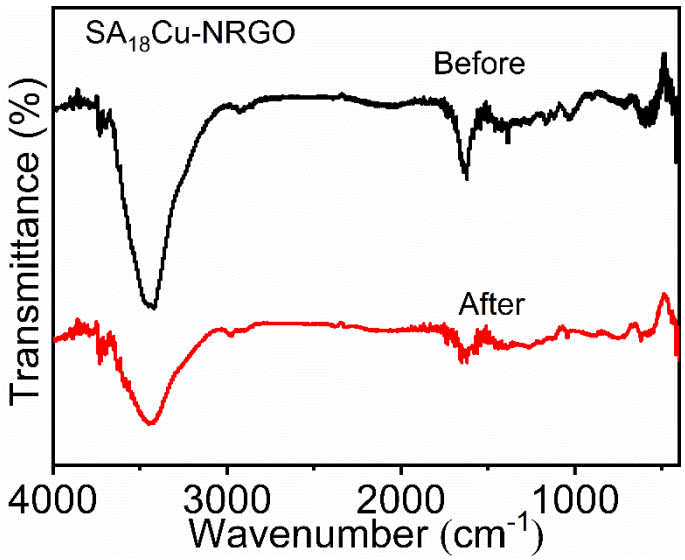

Fig. S12. FTIR spectra before and after the oxidation of benzene.

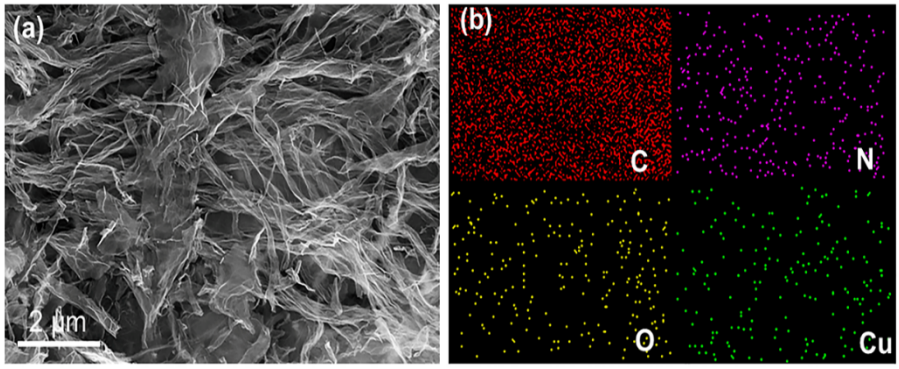

Fig. S13. Mapping images of $SA_{18}Cu$-NRGO after the oxidation of benzene.

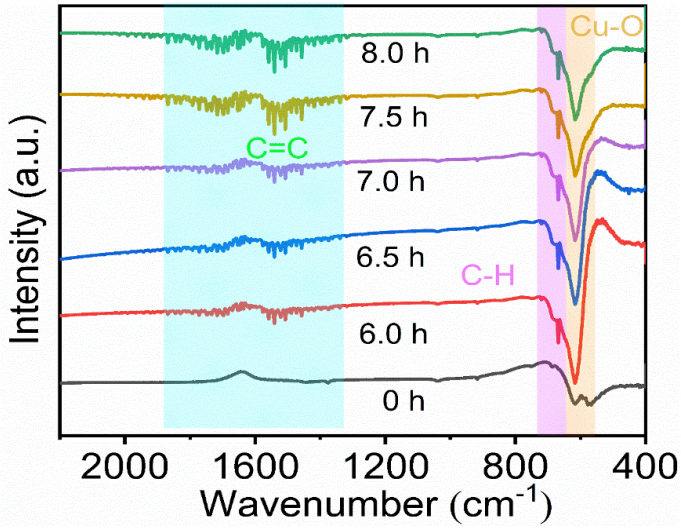

Fig. S14. In situ FTIR spectra of SA_{18}Cu-NRGO in the oxidation of benzene process.

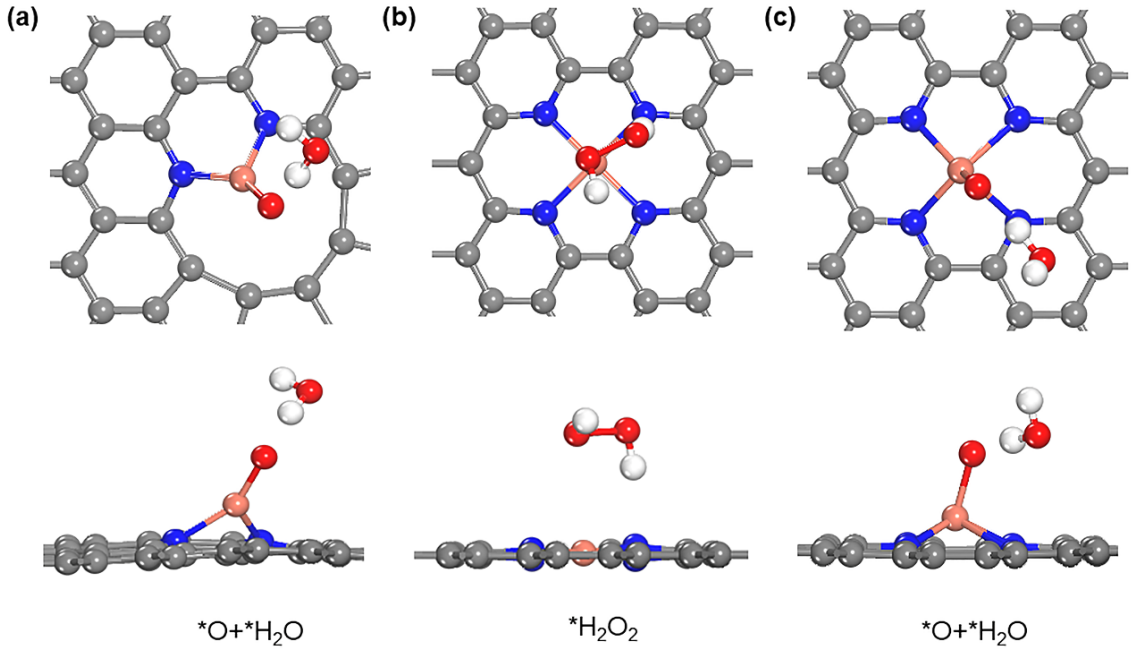

Fig. S15. Optimized configures of H_2O_2 activation on CuN_2 site (a) and CuN_4 site (b and c): (a) direct dissociative adsorption of H_2O_2 on CuN_2, (b) adsorption of H_2O_2 on CuN_4 center, and (c) generated O species with a weak hydrogen bond linked water molecule on CuN_4 center. Where the gray, blue, red, magenta and white balls represent C, N, O, Cu and H atoms, respectively.

Table S1. TG results of all as–prepared samples

Samples	$TG_{Weight\ loss}$ (wt %)	$TG_{Remain\ weight}$ (wt %)	TG_{CuO} (wt %)	TG_{Cu} (wt %)
NRGO	94.06	5.94	0	0
SA_0Cu–NRGO	95.22	4.78	/	/
SA_3Cu–NRGO	92.77	7.23	1.29	1.03
SA_6Cu–NRGO	91.81	8.19	2.25	1.80
SA_9Cu–NRGO	89.85	10.15	4.21	3.37
$SA_{12}Cu$–NRGO	87.96	12.04	6.10	4.88
$SA_{15}Cu$–NRGO	87.77	12.23	6.29	5.03
$SA_{18}Cu$–NRGO	87.13	12.87	6.93	5.54
$SA_{21}Cu$–NRGO	89.01	10.99	5.05	4.04

$TG_{Weight\ loss}$ is the mass ratio of the sample lost in the air atmosphere at 800 °C, and $TG_{Remain\ weight}$ is the remaining mass ratio ($TG_{Remain\ weight}$ =100 – $TG_{Weight\ loss}$ (wt%)). TG_{CuO} is the mass fraction of CuO after the sample is calcined in air atmosphere at 800 °C (TG_{CuO} = $TG_{Remain\ weight}$ − $TG_{Remain\ weight(NRGO)}$ (wt%)). Finally, the mass fraction of Cu (TG_{Cu}) in the sample is calculated like this $TG_{Cu} = TG_{CuO} \times M_{Cu}/(M_{Cu} + M_O)$ (wt%).

Table S2. Textural properties of all as-prepared samples

Samples	S_{BET} (m^2/g)	Vp [a] (cm^3/g)	D_p [b] (nm)
SA_0Cu-NRGO	24.0	0.06	15.3
SA_3Cu-NRGO	56.7	0.24	13.3
SA_6Cu-NRGO	59.2	0.21	14.7
SA_9Cu-NRGO	59.4	0.20	14.0
SA_{12}Cu-NRGO	67.8	0.20	11.7
SA_{15}Cu-NRGO	68.1	0.23	13.3
SA_{18}Cu-NRGO	78.9	0.29	14.6
SA_{21}Cu-NRGO	84.7	0.40	16.0

[a] Pore volume measured at the single point of P/P_0 =0.99

[b] BJH desorption average pore diameter.

Table S3. Structural parameters of $SA_{18}Cu$-NRGO extracted from the EXAFS fitting.

Active site	CN	*R*(Å)	$\sigma^2(10^{-3}Å^2)$	ΔE_0(eV)	*R* factor	S_0^2
CuN_3	3.0±0.5	1.92±0.02	10.0±0.2	7.6±0.4	0.004	0.986
CuN_2	1.8±0.2	1.91±0.01	8.1±0.2	6.2±1.4	0.011	1.255
CuN_4	3.87±0.5	1.92±0.02	7.2±0.2	7.2±1.5	0.032	0.581

S_0^2 is the amplitude reduction factor; CN is the coordination number; *R* is interatomic distance (the bond length between central atoms and surrounding coordination atoms); σ^2 is Debye-Waller factor (a measure of thermal and static disorder in absorber-scatter distances); ΔE_0 is edge-energy shift (the difference between the zero kinetic energy value of the sample and that of the theoretical model). *R* factor is used to value the goodness of the fitting.

Table S4. Comparison of the catalytic performance of $SA_{18}Cu$-NRGO with catalysts reported in literatures on the oxidation of benzene.

Catalyst	Time (h)	Temp (°C)	Benzene Conversion (%)	Selectivity of phenol (%)	Ref.
$SA_{18}Cu$-NRGO	24	25	16.1	98.6	This work
$Fe/Pt/TiO_2$	4	30	6.5	91	2
V/MCM-41	6	60	1.4	93	3
Fe/SBA-16	8	65	12.1	96	4
Fe_3O_4/CMK-3	4	60	18.0	92	5
$FeCl_3$/eg-C_3N_4	3	60	22.0	99	6
$Fe_5V_{2.5}Cu_{2.5}/TiO_2$	4	30	9.8	73	7
$CuO\text{-}Cr_2O_3$	12	80	28.2	75	8
$FeSO_4$	1	25	8.6	97	9
Re@DWNT	5	80	10.2	99	10
Cu-SA/HCNS	24	25	33.4	91	11
Cu_1N_2/HCNS	12	60	70.9	91.3	12
Cu_1N_3/HCNS	12	60	15.6	99.3	12
ISAS Fe/NPC	24	60	42	99	13
ISAS Co/NPC	24	60	26	99	13
ISAS Ni/NPC	24	60	7.1	99	13
Cu_1/NC-1000	1	60	82	96	14
FeN_4	24	30	78.4	100	15
FeN_4-GN	24	25	23.4	80	16
Cu SAC/S−N	24	25	42.3	93.4	17

REFERENCES

1 W. S. Hummers and R. E. Offeman, Preparation of graphitic oxide, *J. Am. Chem. Soc.*, 1958, 80(6), 1339.

2 G. Tanarungsun, W. Kiatkittipong, P. Praserthdam, H. Yamada, T. Tagawa and S. Assabumrungrat, Hydroxylation of benzene to phenol on Fe/TiO_2 catalysts loaded with different types of second metal, *Catal. Commun.*, 2008, **9**, 1886–1890.

3 C. W. Lee, W. J. Lee, Y. K. Park and S. E. Park, Catalytic hydroxylation of benzene over vanadium-containing molecular sieves, *Catal. Today*, 2000, **61**, 137–141.

4 M. Jourshabani, A. Badiei, Z. Shariatinia, N. Lashgari and G. Mohammadi Ziarani, Fe-supported SBA-16 type cagelike mesoporous silica with enhanced catalytic activity for direct hydroxylation of benzene to phenol, *Ind. Eng. Chem. Res.*, 2016, **55**, 3900–3908.

5 P. Arab, A. Badiei, A. Koolivand and G. Mohammadi Ziarani, Direct hydroxylation of benzene to phenol over Fe_3O_4 supported on nanoporous carbon *Chinese J. Catal.*, 2011, **32**, 258–263.

6 Z. Yu, Y. Gan, J. Xu and B. Xue, Direct catalytic hydroxylation of benzene to phenol catalyzed by $FeCl_3$ supported on exfoliated graphitic carbon nitride, *Catal. Letters*, 2020, **150**, 301–311.

7 G. Tanarungsun, W. Kiatkittipong, P. Praserthdam, H. Yamada, T. Tagawa and S. Assabumrungrat, Ternary metal oxide catalysts for selective oxidation of benzene to phenol, *J. Ind. Eng. Chem.*, 2008, **14**, 596–601.

8 S. S. Acharyya, S. Ghosh, S. Adak, T. Sasaki and R. Bal, Facile synthesis of $CuCr_2O_4$ spinel nanoparticles: a recyclable heterogeneous catalyst for the one pot hydroxylation of benzene *Catal. Sci. Technol.*, 2014, **4**, 4232–4241.

9 D. Bianchi, R. Bortolo, R. Tassinari, M. Ricci and R. Vignola, A novel iron-based catalyst for the biphasic oxidation of benzene to phenol with hydrogen peroxide, *Angew. Chemie. Int. Ed.*, 2000, **39**, 4321–4323.

10 H. Zhang, X. Pan, X. Han, X. Liu, X. Wang, W. Shen and X. Bao, Enhancing chemical reactions in a confined hydrophobic environment: An NMR study of benzene hydroxylation in carbon nanotubes, *Chem. Sci.*, 2013, **4**, 1075–1078.

11 T. Zhang, D. Zhang, X. Han, T. Dong, X. Guo, C. Song, R. Si, W. Liu, Y. Liu and Z. Zhao, Preassembly Strategy to fabricate porous hollow carbonitride spheres inlaid with single Cu-N_3 sites for selective oxidation of benzene to phenol, *J. Am. Chem. Soc.*, 2018, **140**, 16936–16940.

12 T. Zhang, X. Nie, W. Yu, X. Guo, C. Song, R. Si, Y. Liu and Z. Zhao, Single atomic Cu-N_2 catalytic sites for highly active and selective hydroxylation of benzene to phenol, *iScience*, 2019, **22**, 97–108.

13 K. Wu, F. Zhan, R. Tu, W. C. Cheong, Y. Cheng, L. Zheng, W. Yan, Q. Zhang, Z. Chen and C. Chen, Dopamine polymer derived isolated single-atom site metals/N-doped porous carbon for benzene oxidation, *Chem. Commun.*, 2020, **56**, 8916–8919.

14 Q. Shen, P. Li, W. Chen, H. Jin, J. Yu, L. Zhu, Z. Yang, R. Zhao, L. Zheng, W. Song and C. Cao, Ionic-liquid-assisted synthesis of metal single-atom catalysts for benzene oxidation to phenol, *Sci. China Mater.* 2021, **65**, 163–169.

15 Y. Pan, Y. Chen, K. Wu, Z. Chen, S. Liu, X. Cao, W. C. Cheong, T. Meng, J. Luo, L. Zheng, C. Liu, D. Wang, Q. Peng, J. Li and C. Chen, Regulating the coordination structure of single-atom Fe-N_xC_y catalytic sites for benzene oxidation, *Nat. Commun.* 2019, **10**, 1–11.

16 D. Deng, X. Chen, L. Yu, X. Wu, Q. Liu, Y. Liu, H. Yang, H. Tian, Y. Hu, P. Du, R. Si, J. Wang, X. Cui, H. Li, J. Xiao, T. Xu, J. Deng, F. Yang, P. N. Duchesne, P. Zhang, J. Zhou, L. Sun, J. Li, X. Pan and X. Bao, A single iron site confined in a graphene matrix for the catalytic oxidation of benzene at room temperature, *Sci. Adv.*, 2015, e1500462.

17 H. Zhou, Y. Zhao, J. Gan, J. Xu, Y. Wang, H. Lv, S. Fang, Z. Wang, Z. Deng, X. Wang, P. Liu, W. Guo, B. Mao, H. Wang, T. Yao, X. Hong, S. Wei, X. Duan, J. Luo and Y. Wu, Cation-exchange induced precise regulation of single copper

site triggers room-temperature oxidation of benzene, *J. Am. Chem. Soc.*, 2020, **142**, 12643–12650.